Negative Sequence Control for Virtual Synchronous Machines Under Unbalanced Conditions

Eros B. Avdiaj, Salvatore D'Arco, Luigi Piegari, *Senior Member, IEEE,* and Jon Are Suul, *Member, IEEE*

***Abstract* – In this paper, five strategies for controlling the negative sequence currents of a Virtual Synchronous Machine (VSM) under unbalanced conditions are comparatively assessed, considering both grid-connected and islanded operation. While these strategies have been individually proposed in recent literature, their characteristics and performance have not previously been systematically evaluated. Thus, a VSM structure serving as basis for the comparison is presented in detail, with modifications for preventing double frequency power oscillations from influencing the virtual swing equation and the inertial dynamics. The active and reactive power oscillations, and the power transfer capability within the converter current limitation, are theoretically derived as a function of the unbalances in the local voltage. Simulation results and experimental validation on a 50 kVA Modular Multilevel Converter (MMC) prototype with 12 sub-modules per arm demonstrate the validity of the theoretical analysis. The presented results serve as basis for evaluating the applicability of the studied control strategies under different operating conditions.**

***Index Terms*—Grid-forming Control, High Voltage Direct Current Transmission, Islanded Operation, Modular Multilevel Converters, Positive and Negative Sequence Components, Negative Sequence Current Control, Power Transfer Capability Unbalanced Three Phase Systems, Virtual Impedance, Virtual Synchronous Machines**

Manuscript received, November 2, 2021; revised January 28, 2022 and March 21, 2022; accepted, April 20, 2022. Date of publication xx yy, 2022; date of current version xx, yy 2022. This work was conducted within the project "HVDC Inertia Provision" (HVDC Pro), supported by the ENERGIX program of the Research Council of Norway (RCN) under project number 268053/E2, and the industry partners; Statnett, Statoil, RTE and ELIA. Recommended for publication by Associate Editor nn. *(Corresponding author: Jon Are Suul.)*

E. B. Avdiaj was with the Department of Electronics, Information and Bioengineering, Politecnico di Milano, 20133 Milan, Italy, and is now with the Department of Electrical Engineering (ESAT-ELECTA), KU Leuven & EnergyVille, 3001 Leuven & 3600 Genk, Belgium (e-mail: eros.avdiaj@kuleuven.be).

S. D'Arco is with SINTEF Energy Research, 7465 Trondheim, Norway (e-mail: salvatore.darco@sintef.no).

L. Piegari is with the Department of Electronics, Information and Bioengineering, Politecnico di Milano, 20133 Milan, Italy (e-mail: luigi.piegari@polimi.it).

J. A. Suul is with SINTEF Energy Research, 7465 Trondheim and also with the Department of Engineering Cybernetics, Norwegian University of Science and Technology, 7491 Trondheim, Norway (e-mail: Jon.A.Suul@sintef.no).

Color versions of one or more of the figures in this article are available online at https://ieeexplore.ieee.org.

Digital Object Identifier

NOMENCLATURE

Main variables and parameters

Upper case symbols represent quantities in the SI system
Lower case symbols represent per unit quantities
Bold fonts represent complex or space vector quantities

V	Voltage
I	Current
P, Q	Active, Reactive power
W	Energy
R, L, C, X	Resistance, Inductance, Capacitance, Reactance
ω	Angular frequency (in per unit quantities)
θ	Phase angle

Main control system parameters

T_a	Inertia time constant
k_ω	Frequency droop gain
k_d	Damping coefficient
k_q	Reactive power droop gain

Subscripts

a, b, c, k	Phases a,b and c or unspecified phase k
b	Base value for per unit system
e	Equivalent voltage behind a virtual impedance
o	Output terminals at the point of common coupling (PCC)
v	Converter ac side quantities
g	Grid parameters
VSM	Virtual synchronous machine
VI	Virtual impedance
PLL	Phase Locked Loop
T	Transformer parameters
dc	Direct current component
$s2, c2$	Sine and cosine terms in second harmonic oscillations
dq	Synchronous reference frame direct and quadrature axis components
$\alpha\beta$	Stationary frame orthogonal components
z	Zero sequence component

Superscripts

$+,-, z$	Positive, Negative, Zero sequence component
dc	DC component
ω	Fundamental frequency component
$2\,\omega$	Second harmonic component
PI	Term resulting as output of a PI regulator
*	Reference value for control

Symbol modifiers

$\hat{\square}$	Amplitude of three phase quantity or oscillating component
$\lvert\square\rvert$	Absolute value of complex vector quantities
$\overline{\square}$	Average value

I. INTRODUCTION

The increasing utilization of converter-interfaced generation and the associated reduction in the share of conventional synchronous generators are leading to concerns regarding declining inertia and stability margins in traditional power systems [1]-[4]. Related challenges associated with the

need for "grid-forming" control of power electronic converters in stand-alone applications and small-scale microgrids without synchronous generators have been widely studied over the last decades [5], [6]. However, the ongoing development has the potential for leading to a dominant presence of power electronic converters also in large-scale transmission systems. Therefore, Transmission System Operators (TSOs) are currently directing significant attention to the development of "grid-forming" functionalities from power electronic converters [7]-[10]. In this context, the operation of Voltage Source Converter (VSC) HVDC terminals as "grid-forming" units or for providing virtual inertia can be especially relevant due to their controllability and high power rating [7], [9]-[14].

A major requirement for converters with "grid-forming" capability is that they should be able to define their local grid voltage [5], [7], [10]. Thus, "grid-forming" control strategies cannot depend on voltage measurement-based synchronization to the phase angle of an external voltage. One specific class of control strategies that can fulfill this requirement is associated with the concept of Virtual Synchronous Machines (VSMs), which has been introduced with various implementations for a wide range of applications during the last 15 years [15]-[20]. By explicitly emulating the inertial dynamics and power-balance-based synchronization mechanism of a synchronous machine (SM), a VSM-controlled converter inherently provides "grid-forming" functionalities as well as virtual inertia support to the power system.

The general operation of a converter as a "grid-forming" unit would also require the ability to respond seamlessly to all potential operating conditions, including islanded operation with unbalanced loads and operation under balanced or unbalanced grid faults. Although most studies of VSM-based control have assumed balanced three phase conditions, several recent publications have addressed the challenges of adapting VSM implementations to the operation under unbalanced conditions. For instance, a strategy for obtaining balanced three-phase currents from a VSM under unbalanced grid faults is presented in [21]. Implementations of flexible approaches for controlling a VSM to achieve balanced three phase currents, elimination of active power oscillations or elimination of reactive power oscillations are also discussed in [22]-[28]. Furthermore, a VSM implementation utilizing a negative sequence virtual impedance for operation under unbalanced grid faults has been demonstrated in [29].

A flexible control for grid connected operation with an additional option of generating balanced three phase voltages under islanded conditions with unbalanced loads was introduced in [25]. Similarly, a closed loop control for providing negative sequence current references that eliminates the negative sequence voltage components when supplying an unbalanced islanded load is described in [30]. Finally, a unified implementation allowing for selecting between all these general strategies for controlling the negative sequence currents was presented in [31], supported by a comparative evaluation of the performances in grid connected and islanded conditions. However, all these studies have been conducted for 2-level VSCs operated as VSMs. Furthermore, except from the preliminary results in [31], no comparative evaluation or comprehensive analysis of the different strategies within a common framework has been presented.

To address the limitations of the existing literature, this paper systematically evaluates five different strategies for controlling the negative sequence currents of a VSM during unbalanced conditions. These strategies include control for ensuring balanced positive sequence currents, elimination of double frequency active or reactive power oscillations, operation with a negative sequence virtual impedance, or closed loop negative sequence voltage control for eliminating voltage unbalances. Furthermore, a common implementation framework is presented, and the analysis of the studied strategies is validated by simulations and experimental results. Thus, the main contributions can be summarized as:

i. Analytical investigation of how the different strategies for controlling the negative sequence currents of a VSM influences the power flow characteristics during unbalanced conditions. The power transfer capability within a certain current limitation is also derived for the different evaluated control strategies.
ii. A comprehensive comparative assessment of the five evaluated strategies for controlling a VSM under unbalanced conditions. The evaluation is conducted for both grid connected and islanded operation.

The presented analysis and discussions are applicable to any VSM-controlled VSC topology. However, the operational characteristics of the studied control strategies are validated by simulation of an HVDC scale Modular Multilevel Converter (MMC) as well as by laboratory experiments with a small-scale MMC prototype. The presented results provide a comprehensive basis for comparative assessment of the evaluated VSM-based control strategies. Thus, the performance and applicability of the different control strategies for grid-connected and islanded operation of the VSM is evaluated, leading to an overview of what control strategies are most suitable for different conditions. For the case of an MMC-controlled VSM, operation with balanced positive sequence currents or elimination of reactive power oscillation are shown to be suitable options for grid connected operation. Furthermore, operation with closed loop negative sequence voltage control is mainly relevant for operation in islanded conditions or in very weak grid conditions. However, the only strategy that is directly applicable in both grid-connected and islanded conditions is operation with a negative sequence virtual impedance.

II. OVERVIEW OF VSM-BASED CONTROL UNDER UNBALANCED CONDITIONS

An overview of the configuration considered in this paper for evaluating VSM-based control strategies under unbalanced conditions is shown in Fig. 1. A local load is connected at the point of common coupling (PCC) and will be supplied by the VSM during islanded operations.

The analysis of the general ac-side operation of the VSM can be largely considered independent of the converter topology. However, an MMC and the corresponding control

This article has been accepted for publication in a future issue of this journal, but has not been fully edited. Content may change prior to final publication. Citation information: DOI 10.1109/JESTPE.2022.3175169, IEEE Journal of Emerging and Selected Topics in Power Electronics

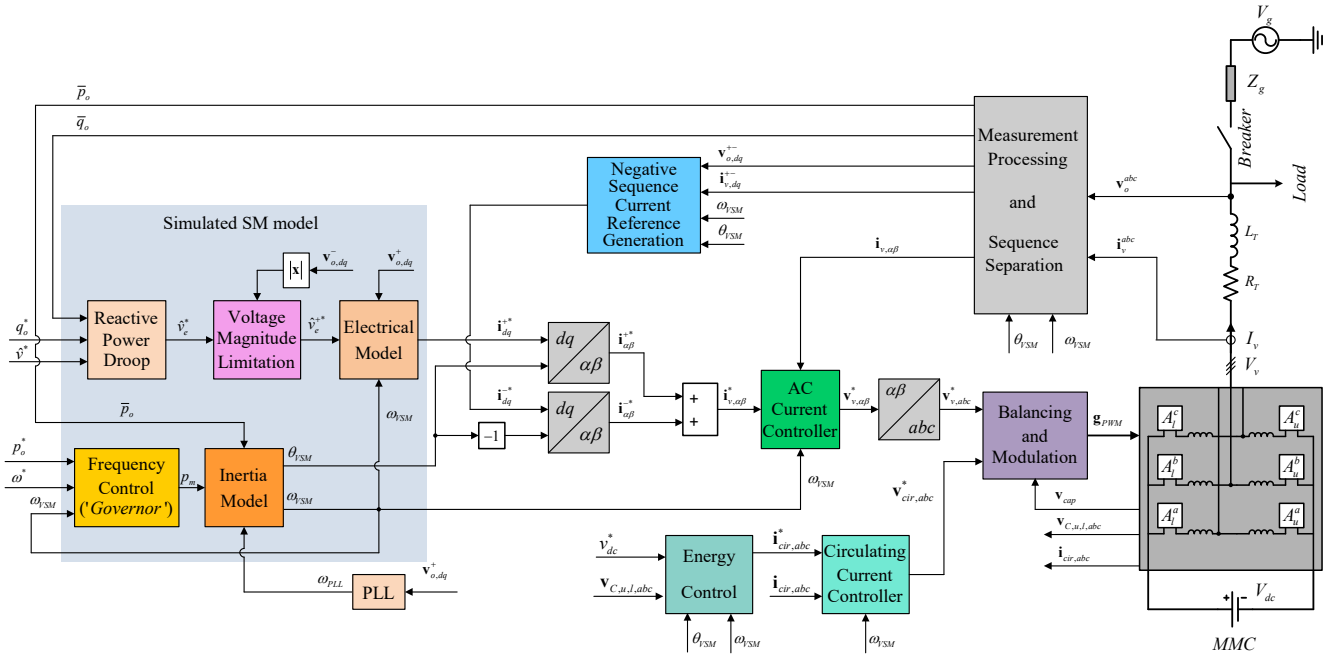

Fig. 1 Overview of VSM-based control strategy for operation under unbalanced conditions

loops is indicated in Fig. 1, since the simulations and experiments in this paper are based on this topology. Thus, the converter is connected to the ac grid by means of an impedance defined by L_T and R_T (which could represent the series impedance of a transformer) and a breaker. However, operation with a 2-level VSC would typically require an LCL-filter.

As shown in Fig. 1, the gate signals for controlling the individual modules in each arm of the MMC are generated to follow a voltage reference while balancing the capacitor voltages according to [32], [33]. The inputs to the control block representing the balancing and modulation are the reference signals for the voltages driving the ac-side currents and the circulating currents [34]. These voltage signals are generated separately by an ac-side current controller and a circulating current controller. The ac-side current references consist of a positive sequence component and a negative sequence component that are provided by the electrical model of the VSM-based control strategy and generated to shape the response to the unbalances, respectively. The circulating current references are generated by outer loop energy controllers developed from [34], [35], as further documented in [36]. The electrical configuration and the individual control blocks are described in more detail in the following sections.

A. *Sequence separation and power calculation under unbalanced conditions*

Under unbalanced conditions the magnitudes of the voltage and current vectors, as well as the instantaneous active and reactive power flow, present oscillations at twice the fundamental frequency. In this paper, voltage and current measurements are separated into positive and negative sequence components by the use of a Dual Second Order Generalized Integrator configured for Quadrature Signal Generation (DSOGI-QSG) according to [37]. The DSOGI-QSG generates the in-phase and in-quadrature signals required for the positive and the negative sequence calculations (PNSC). However, differently from [37], frequency adaptivity is achieved by using the VSM speed as input to the DSOGI-QSGs instead of a frequency estimation based on the voltage measurements.

By obtaining the positive and negative sequence components of the measured voltages and currents, it is possible to isolate the oscillating terms and the constant terms of the active and reactive power [38]. The constant terms, $\bar{p}_o$ and $\bar{q}_o$, also referred to as average values or dc-components, are calculated in per unit quantities as

$$\begin{aligned}\bar{p}_o &= v^+_{o,\alpha}\cdot i^+_{v,\alpha} + v^+_{o,\beta}\cdot i^+_{v,\beta} + v^-_{o,\alpha}\cdot i^-_{v,\alpha} + v^-_{o,\beta}\cdot i^-_{v,\beta} \\ \bar{q}_o &= -v^+_{o,\alpha}\cdot i^+_{v,\beta} + v^+_{o,\beta}\cdot i^+_{v,\alpha} - v^-_{o,\alpha}\cdot i^-_{v,\beta} + v^-_{o,\beta}\cdot i^-_{v,\alpha}\end{aligned} \quad (1)$$

These average active and reactive power components are then used as feedback signals in the VSM-based control as indicated in Fig. 1. Instead of feeding back the instantaneous active and reactive power signals as in [21], [24], this approach avoids the influence from double frequency oscillations on the virtual swing equation and the reactive power droop [31].

B. *VSM-based generation of positive sequence current references*

The evaluated VSM-based control strategies synchronize to the positive sequence component of the ac voltage by responding to the dc-component of the active power flow, while the ac voltage or reactive power control is based on the dc-component of the reactive power flow. The control scheme

This article has been accepted for publication in a future issue of this journal, but has not been fully edited. Content may change prior to final publication. Citation information: DOI 10.1109/JESTPE.2022.3175169, IEEE Journal of Emerging and Selected Topics in Power Electronics

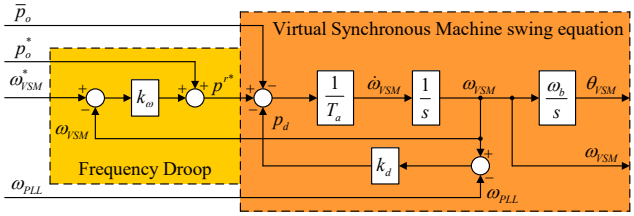

Fig. 2 Inertia model implemented by a virtual swing equation and operated with an ideal frequency droop as a 'governor' function

includes a simplified SM model, which reproduces the inertial behaviour and the quasi-stationary effect of the equivalent stator impedance. The implementation of these control functions is adapted from [39], [40] and [31].

1) Inertia emulation and active power droop

The inertia emulation and grid synchronization mechanism of the VSM is provided by a virtual swing equation as shown in the right-hand side of Fig. 2 [20]. The swing equation is linearized with respect to the VSM speed, ω_{VSM}, so that the power balance directly gives the acceleration of the inertia. Moreover, the frequency droop emulating the steady-state characteristics of a traditional "governor" for a synchronous machine is represented in the left-hand side of Fig. 2 [40]. Thus, the dynamic equation representing the VSM speed can be expressed as

$$T_a \frac{d\omega_{VSM}}{dt} = k_\omega \left(\omega^*_{VSM} - \omega_{VSM}\right) + k_d \left(\omega_{VSM} - \omega_{PLL}\right) + p^*_o - \bar{p}_o, \quad (2)$$

where T_a is the mechanical time constant, and k_ω is the droop gain acting on the difference between the frequency reference ω^*_{VSM} and ω_{VSM}. The internal damping power of the virtual swing equation is defined by the damping coefficient k_d and the difference between ω_{VSM} and the grid frequency, ω_{PLL}, provided by a phase locked loop (PLL) [40]. In this case, the grid frequency detection by the PLL is based on the positive sequence component of the measured voltage [31]. Finally, p_o^* is the external power set-point for the VSM swing equation.

The phase angle θ_{VSM} is resulting from integration of ω_{VSM} and is used for transformations between the stationary reference frame and the positive sequence dq frame in the control system. Furthermore, $-\theta_{VSM}$ is used for transformation to or from the negative sequence dq frame. It should also be noted that the phase angle δ_{VSM} between the reference frame defined by the VSM and the orientation of the positive sequence voltage $\mathbf{v}_o^+$ can be expressed as

$$\delta_{VSM} = \int \omega_b \left(\omega_{VSM} - \omega_g\right) dt = \theta_{VSM} - \theta_g^+, \quad (3)$$

where ω_g is the grid frequency and θ^+_g is the phase angle of the positive sequence input voltage component $\mathbf{v}_o^+$.

2) Electrical model

To emulate the stator impedance of the synchronous machine, a quasi-stationary electrical model is implemented according to [39]. It is worth to highlight that this electrical model is not representative of any real physical system and is not affected by parameter uncertainties or need for a prior system identification. As discussed in [24], [31], this virtual impedance is only applied to the positive sequence components. Thus, the positive sequence current reference $\mathbf{i}_v^+ = i_{v,d}^+ + j\, i_{v,q}^+$ is calculated as

$$\mathbf{i}_v^+ = \frac{\hat{v}_e^{+*} - \mathbf{v}_o^+}{r_{VI}^+ + j\omega_{VSM} l_{VI}^+}, \quad (4)$$

where $\hat{v}_e^{+*}$ is the internal positive sequence voltage amplitude provided by the reactive power control and an internal voltage amplitude limitation. Furthermore, $\mathbf{v}_o^+$ is the positive sequence component of the measured voltage represented in the positive sequence dq reference frame defined by the virtual swing equation. The positive sequence virtual resistance and inductance are given by r_{VI}^+ and l_{VI}^+, respectively, while the frequency dependency of the reactance is ensured by a multiplication with the VSM speed. It should be noted that the positive sequence current references can be limited to safe values at the input to the current controllers without interfering with the virtual impedance.

3) Voltage reference limitation and reactive power droop

From (4), it can be understood that a high value of $\hat{v}_e^{+*}$ combined with a drop in the positive sequence grid voltage will lead to a high reactive current flowing in the virtual impedance of the VSM, and a correspondingly high reactive power flow to the grid. Furthermore, under unbalanced conditions, reactive power injection for increasing the positive sequence voltage component can lead to over-voltage in the phase(s) with high remaining voltage (i.e. resulting in $|\mathbf{v}_o^+|+|\mathbf{v}_o^-|>1$). In order to avoid such over-voltages, the internal positive sequence voltage magnitude is limited in relation to the amplitude of the negative sequence voltage by

$$0 < \hat{v}_e^{+*} < k_{v,\lim} \cdot (1 - |\mathbf{v}_o^-|), \quad (5)$$

where $k_{v,\lim}$ is the voltage limiting factor. Thus, $k_{v,\lim}$ can be selected depending on the virtual impedance to ensure that the voltage reference is kept within a range that will provide a reasonable maximum reactive current.

When the limitation in (5) is not active, the internal voltage reference for the VSM is given by a reactive power droop. Thus, $\hat{v}_e^{*+}$ is then calculated as

$$\hat{v}_e^{*+} = \hat{v}_e^* = \hat{v}^* + k_q \left(q_o^* - \bar{q}_o\right), \quad (6)$$

where $\hat{v}^*$ is the external reference for the voltage amplitude, q_o^* is the reactive power reference, $\bar{q}_o$ is the average reactive power flow according to (1) and k_q is the reactive power droop coefficient [31]. Alternatively, a closed loop voltage control could be introduced after the reactive power droop, as applied in [39]. However, this would imply the need for anti-windup protection of the controller when the limitation in (5) is active, and is not further discussed in the following.

III. STRATEGIES FOR NEGATIVE SEQUENCE CURRENT CONTROL

While the implementation presented in section II. provides a general VSM-based strategy for the control of the positive sequence components, there are several options for controlling the negative sequence quantities in response to unbalances in the ac-grid. Thus, several different strategies for operation under unbalanced conditions can be obtained by considering different objectives for the Negative Sequence Current Reference Generation (NSCRG) indicated in Fig. 1. For understanding and assessing the different strategies for controlling the negative sequence currents, it is useful to start

This article has been accepted for publication in a future issue of this journal, but has not been fully edited. Content may change prior to final publication. Citation information: DOI 10.1109/JESTPE.2022.3175169, IEEE Journal of Emerging and Selected Topics in Power Electronics

from the definition of the six different power flow components that can be identified under unbalanced conditions [24], [38], as given by

$$\begin{bmatrix} \bar{p}_o \\ p_{c2\omega} \\ p_{s2\omega} \\ \bar{q}_o \\ q_{c2\omega} \\ q_{s2\omega} \end{bmatrix} = \begin{bmatrix} v^+_{o,d} & v^+_{o,q} & v^-_{o,d} & v^-_{o,q} \\ v^-_{o,d} & v^-_{o,q} & v^+_{o,d} & v^+_{o,q} \\ v^-_{o,q} & -v^-_{o,d} & -v^+_{o,q} & v^+_{o,d} \\ v^+_{o,q} & -v^+_{o,d} & v^-_{o,q} & -v^-_{o,d} \\ v^-_{o,q} & -v^-_{o,d} & v^+_{o,q} & -v^+_{o,d} \\ -v^-_{o,d} & -v^-_{o,q} & v^+_{o,d} & v^+_{o,q} \end{bmatrix} \begin{bmatrix} i^+_{v,d} \\ i^+_{v,q} \\ i^-_{v,d} \\ i^-_{v,q} \end{bmatrix}. \quad (7)$$

In these expressions, $\bar{p}_o$ and $\bar{q}_o$ correspond to (1), although calculated from current and voltage components defined in the positive and negative sequence synchronous reference frames [24], [38]. The other active and reactive power components in (7) represent the amplitude of double frequency oscillations, where $p_{c2\omega}$ and $q_{c2\omega}$ are components depending on cosine terms while $p_{s2\omega}$ and $q_{s2\omega}$ are components depending on sine terms. It should be noted that (7) identifies six unique power components, while there are only four controllable current components (i.e. the *d*- and *q*-axis components of the positive and negative sequence currents). Thus, only four of the defined power components can be explicitly controlled. Furthermore, since $i^+_{v,d}$ and $i^+_{v,q}$ will be generated by (4) with a phase orientation resulting from the virtual swing equation in (2), $\bar{p}_o$ will settle to p_o^* in steady state, while $\bar{q}_o$ will be implicitly defined by $\hat{v}_e^{+*}$. Therefore, only two of the oscillating power components can be directly controlled by selecting the negative sequence current references. However, the negative sequence current references can also be selected to obtain other objectives. In the following, five different strategies for generating the negative sequence current references are introduced and evaluated.

A. Balanced Positive Sequence Current (BPSC) control

The simplest approach for controlling the VSM operation under unbalanced conditions is to set the negative sequence current references to zero. Thus, the strategy for providing Balanced Positive Sequence Currents (BPSC) can be directly defined by [24], [31], [38]

$$\mathbf{i}^{-*}_{BPSC} = \begin{bmatrix} i^{-*}_d \\ i^{-*}_q \end{bmatrix}_{BPSC} = \begin{bmatrix} 0 \\ 0 \end{bmatrix}. \quad (8)$$

This strategy ensures that the VSM can operate with balanced currents independently of unbalances in the ac-grid. However, it can be seen directly from (7) that the interactions between the balanced positive sequence currents and a negative sequence voltage component will cause oscillations in both the active and reactive power flow. Considering that the sine and cosine terms in (7) are 90° phase shifted, the amplitude of the active and reactive power oscillations can be calculated as $\hat{p}_{2\omega} = \sqrt{p^2_{c2\omega} + p^2_{s2\omega}}$ and $\hat{q}_{2\omega} = \sqrt{q^2_{c2\omega} + q^2_{s2\omega}}$, respectively. Furthermore, the positive sequence current components corresponding to a certain average active and reactive power flow given by $\bar{p}_o$ and $\bar{q}_o$ can be calculated from (7) as a function of the voltage components. Then, by substituting the resulting positive sequence current components into the equations for $p_{c2\omega}$, $p_{s2\omega}$, $q_{c2\omega}$, and $q_{s2\omega}$, the amplitude of the oscillating components can be derived as

$$\hat{p}_{2\omega,BPSC} = \hat{q}_{2\omega,BPSC} = \frac{\left|\mathbf{v}^-_o\right|}{\left|\mathbf{v}^+_o\right|} \cdot \sqrt{\bar{p}_o^{\,2} + \bar{q}_o^{\,2}}\,. \quad (9)$$

It can be seen from (9) that the active and reactive power oscillations for a given combination of average active and reactive power flow is proportional to the amplitude of the negative sequence voltage and inversely proportional to the positive sequence voltage amplitude.

B. Constant Active Power (CAP) control

As discussed in [22]-[24], [31], the negative sequence currents of a VSM can be controlled to eliminate the double frequency oscillations in the active power flow. This can be achieved by setting p_{c2} and p_{s2} in (7) to zero and solving the two corresponding equations for $i^-_{v,d}$ and $i^-_{v,q}$. The resulting expressions allow for calculating the negative sequence current references from the positive sequence currents and the measured positive and negative sequence voltage components:

$$\mathbf{i}^{-*}_{CAP} = \begin{bmatrix} i^{-*}_d \\ i^{-*}_q \end{bmatrix}_{CAP} = \frac{-1}{(v^+_{o,d})^2 + (v^+_{o,q})^2} \cdot \begin{bmatrix} v^+_{o,d}v^-_{o,d} - v^+_{o,q}v^-_{o,q} & v^+_{o,q}v^-_{o,d} + v^+_{o,d}v^-_{o,q} \\ v^+_{o,q}v^-_{o,d} + v^+_{o,d}v^-_{o,q} & v^+_{o,q}v^-_{o,q} - v^+_{o,d}v^-_{o,d} \end{bmatrix} \begin{bmatrix} i^+_{v,d} \\ i^+_{v,q} \end{bmatrix}. \quad (10)$$

While this expression ensures elimination of the active power oscillations, the amplitude of the reactive power oscillations will increase with the power flow and voltage unbalance. By introducing the expressions from (10) into the equations for $q_{c2\omega}$ and $q_{s2\omega}$ in (7), the total amplitude of the reactive power oscillations can be calculated as

$$\hat{q}_{2\omega} = 2 \cdot \left|\mathbf{v}^-_o\right| \cdot \left|\mathbf{v}^+_o\right| \sqrt{\frac{\bar{p}_o^{\,2}}{\left(\left|\mathbf{v}^+_o\right|^2 - \left|\mathbf{v}^-_o\right|^2\right)^2} + \frac{\bar{q}_o^{\,2}}{\left(\left|\mathbf{v}^+_o\right|^2 + \left|\mathbf{v}^-_o\right|^2\right)^2}} \quad (11)$$

It can be noted that the control for eliminating active power oscillations can be especially relevant for 2-level VSCs with small dc-link capacitor, as further discussed in [41]. However, this issue is less critical for the MMC topology, since the internal capacitors in each arm always have to be designed for handling the voltage oscillations corresponding to the maximum allowed phase currents.

C. Constant Reactive Power (CRP) control

The same approach as used for obtaining (10) can also be used to derive the negative sequence current references that will eliminate the double frequency reactive power oscillations during unbalanced conditions. Thus, by setting q_{c2} and q_{s2} in (7) to zero and solving for the negative sequence current components as a function of the voltages and the positive sequence currents, the following expression can be obtained [22]-[24], [31]:

$$\mathbf{i}^{-*}_{CRP} = \begin{bmatrix} i_d^{-*} \\ i_q^{-*} \end{bmatrix}_{CRP} = \frac{1}{(v_{o,d}^{+})^2 + (v_{o,q}^{+})^2} \cdot \begin{bmatrix} v_{o,d}^{+}v_{o,d}^{-} - v_{o,q}^{+}v_{o,q}^{-} & v_{o,q}^{+}v_{o,d}^{-} + v_{o,d}^{+}v_{o,q}^{-} \\ v_{o,q}^{+}v_{o,d}^{-} + v_{o,d}^{+}v_{o,q}^{-} & v_{o,q}^{+}v_{o,q}^{-} - v_{o,d}^{+}v_{o,d}^{-} \end{bmatrix} \begin{bmatrix} i_{v,d}^{+} \\ i_{v,q}^{+} \end{bmatrix} \quad (12)$$

It should be noted that this expression is equal to the expression in (10) multiplied by −1. Then, introducing the negative sequence current components resulting from (12) into (7) results in expressions for the active power oscillations $p_{c2\omega}$ and $p_{s2\omega}$. The amplitude of the active power oscillations can then be expressed as

$$\hat{p}_{2\omega} = 2 \cdot \left|\mathbf{v}_o^{-}\right| \cdot \left|\mathbf{v}_o^{+}\right| \sqrt{\frac{\bar{p}_o^{\,2}}{\left(\left|\mathbf{v}_o^{+}\right|^2 + \left|\mathbf{v}_o^{-}\right|^2\right)^2} + \frac{\bar{q}_o^{\,2}}{\left(\left|\mathbf{v}_o^{+}\right|^2 - \left|\mathbf{v}_o^{-}\right|^2\right)^2}} \quad (13)$$

D. Negative sequence virtual impedance (NSVI) control

While the BPSC, CAP or CRP strategies are designed to impose a specified power flow characteristic to the VSM (i.e. balanced currents, elimination of active power oscillations or elimination of reactive power oscillations), it is also possible to let the VSM respond to unbalanced conditions by a exhibiting a negative sequence virtual impedance (NSVI) [29], [31]. By applying a similar quasi-stationary representation as in (4), a NSVI-based strategy for generating the negative sequence current references can be directly obtained. Expanding the equation for the negative sequence *d*- and *q*-axis components results in:

$$i_d^{-*} = \frac{\left(v_{e,d}^{-*} - v_{o,d}^{-}\right) r_{VI}^{-} - \left(v_{e,q}^{-*} - v_{o,q}^{-}\right) \omega_{VSM} l_{VI}^{-}}{\left(r_{VI}^{-}\right)^2 + \left(\omega_{VSM} l_{VI}^{-}\right)^2},$$
$$i_q^{-*} = \frac{\left(v_{e,q}^{-*} - v_{o,q}^{-}\right) r_{VI}^{-} + \left(v_{e,d}^{-*} - v_{o,d}^{-}\right) \omega_{VSM} l_{VI}^{-}}{\left(r_{VI}^{-}\right)^2 + \left(\omega_{VSM} l_{VI}^{-}\right)^2} \quad (14)$$

By setting the internal negative sequence voltage of the VSM to zero (i.e. $v^{-,*}_{e,d} = v^{-,*}_{e,q} = 0$ in (14)), the generation of the negative sequence current references can be illustrated as shown in the right hand side of Fig. 3. The active and reactive power oscillations resulting from the NVSI-based control can be directly obtained by introducing the currents resulting from (4) and (14) into (7).

The use of a NSVI inherently provides impedance-based sharing of unbalanced load in the system and could thereby contribute to the reduction of the voltage unbalance in the grid, according to the desired requirements for grid forming converters [7]. However, the resulting negative sequence currents will depend on the negative sequence voltage in the grid and on the virtual impedance. Thus, for operation under severe voltage sags, the selection of the negative sequence virtual impedance should be coordinated with the strategy for current limitation and for priority between positive and negative sequence current components, which is outside the scope of this paper.

E. Negative sequence voltage control (NSVC)

A fifth possible strategy is to introduce closed loop control of the negative sequence voltage components measured by the converter [30], [31]. As proposed in [31], such negative sequence voltage control can be obtained by introducing PI-controllers for providing the internal negative sequence *d*- and *q*-axis voltage components $v_{e,d}^{-*}$ and $v_{e,q}^{-*}$ used as input to the NSVI implementation from (14). This is indicated in the left hand side of Fig. 3.

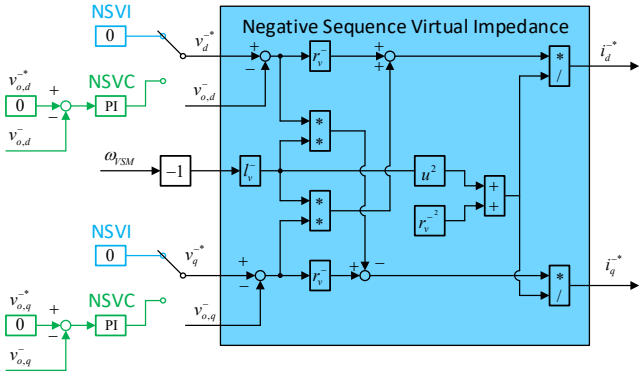

Fig. 3 Block diagram of the NSVI and NSVC

IV. POWER FLOW CHARACTERISTICS AND POWER TRANSFER LIMITATIONS UNDER UNBALANCED CONDITIONS

The ac-side power flow characteristics of the different strategies and the dependency on the grid voltage are studied in the following for all cases of negative sequence current control except the NSVC, which always imposes a balanced local voltage (within its current limitation) Furthermore, the maximum average power that can be transferred within the current limitation of the converter is derived for the different strategies to obtain corresponding ac-side capability curves for the converter.

A. Comparative evaluation of active and reactive power flow characteristics

In the following, the reactive power droop is ignored so that the internal positive sequence voltage amplitude $\hat{v}_e^{+}$ is independent of the converter operation. By representing the positive and negative sequence voltages in the reference frame defined by the VSM, the operating conditions in steady state can then be fully determined. The expressions for the positive sequence components are given as

$$v_{o,d}^{+} = \left|\mathbf{v}_o^{+}\right| \cos\delta_{VSM}, \quad v_{o,q}^{+} = \left|\mathbf{v}_o^{+}\right| \sin\delta_{VSM} \quad (15)$$

The first step of the analysis is to utilize (4), (15) and the expressions for the negative sequence currents from (8), (10), (12) or (14) to eliminate the currents from the equations for the average active and reactive power in (11). Then, $\bar{p}_o$ and $\bar{q}_o$ can be expressed as function of $|\mathbf{v}_o^{+}|$, $|\mathbf{v}_o^{-}|$ and δ_{VSM}. As an example, the expressions for BPSC control are given as:

$$\bar{p}_{o,BPSC} = \left|\mathbf{v}_o^{+}\right| \frac{\omega_{VSM} l_{VI}^{+} \hat{v}_e^{*} \sin\delta_{VSM} + r_{VI}^{+} \hat{v}_e^{*} \cos\delta_{VSM} - r_{VI}^{+} \left|\mathbf{v}_o^{+}\right|}{\left(r_{VI}^{+}\right)^2 + \left(\omega_{VSM} l_{VI}^{+}\right)^2} \quad (16)$$

This article has been accepted for publication in a future issue of this journal, but has not been fully edited. Content may change prior to final publication. Citation information: DOI 10.1109/JESTPE.2022.3175169, IEEE Journal of Emerging and Selected Topics in Power Electronics

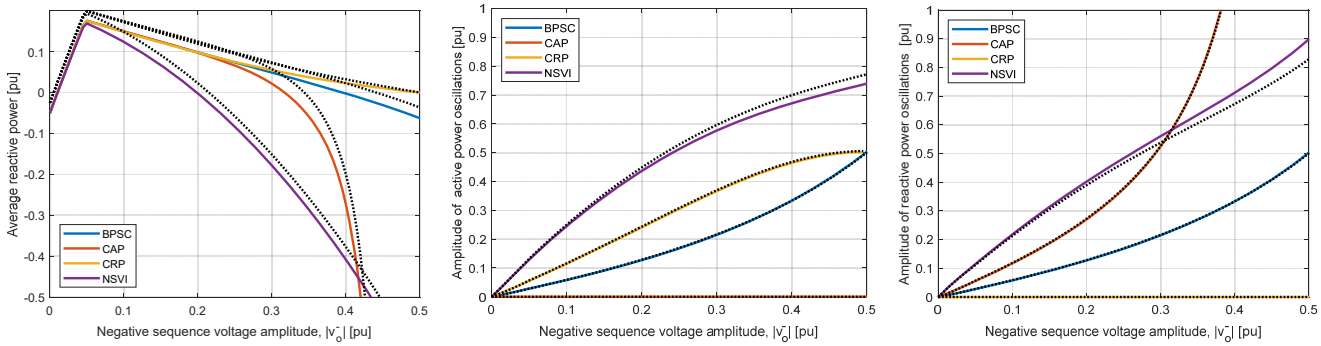

a) Average reactive power flow, $\bar{q}_o$ b) Active power oscillation $\hat{p}_{2\omega}$ c) Reactive power oscillations, $\hat{q}_{2\omega}$

Fig. 4 Calculated power flow characteristics with BPSC, CAP, CRP and NSVI control. Solid lines represent the numerical calculation of the accurate expressions while dotted black lines represent the corresponding simplified expressions obtained with $r_{VI}^{+} = 0$ and $r_{VI}^{-} = 0$, as presented in Appendix A.

$$\bar{q}_{o,BPSC} = \left|\mathbf{v}_o^+\right| \frac{\omega_{VSM} l_{VI}^+ \hat{v}_e^* \cos\delta_{VSM} - r_{VI}^+ \hat{v}_e^* \sin\delta_{VSM} - \omega_{VSM} l_{VI}^+ \left|\mathbf{v}_o^+\right|}{\left(r_{VI}^+\right)^2 + \left(\omega_{VSM} l_{VI}^+\right)^2}, \quad (17)$$

where δ_{VSM} is the only unknown.

Imposing the power flow to be equal to the power reference p_o^*, (16) can be solved for δ_{VSM}. The result can then be used to calculate the average reactive power flow with BPSC as a function of the power reference by (17). The average active and reactive power can be further substituted into (7), or directly into (9), for calculating the amplitudes, $\hat{p}_{2\omega}$ and $\hat{q}_{2\omega}$, of the active and reactive power oscillations. It should be noted that by setting r_{VI}^+ to zero, (16) and (17) simplifies to the basic equation for power transfer between two voltage sources separated by a series inductance. This significantly simplifies the expressions for $\bar{q}_o$, $\hat{p}_{2\omega}$, $\hat{q}_{2\omega}$. Corresponding expressions for the CAP, CRP and NSVI control strategies can also be obtained, as documented in Appendix A.

For comparing the different strategies for negative sequence current control, $\bar{q}_o$, $\hat{p}_{2\omega}$ and $\hat{q}_{2\omega}$ are plotted as a function of the negative sequence voltage amplitude in Fig. 4, a), b) and c), respectively. For these plots, it is assumed that the per unit positive sequence voltage amplitude is given by $|\mathbf{v}_o^+| = 1.0 - |\mathbf{v}_o^-|$, and that the virtual impedances are set to r_{VI}^+=0.01, l_{VI}^+=0.3, r_{VI}^-=0.01, l_{VI}^-=0.4. Furthermore, the voltage reference limitation in (5) is taken into account with $k_{v,lim}$ = 1.05 , by setting $\hat{v}_e^{+*} = 1.05|\mathbf{v}_o^+|$ when $\hat{v}_e^* > 1.05|\mathbf{v}_o^+|$. The effect of this limitation is clearly seen from the plot of $\bar{q}_o$ in Fig. 4 a), as a sudden change of slope. Indeed, without this limitation the reactive power injection would become very high with reduced positive sequence voltage amplitude. The dotted lines show the impact of neglecting the resistances as assumed for the analytic expressions in Appendix A.

The results in Fig. 4 b) and Fig. 4 c) also show how $\hat{p}_{2\omega}$ remains zero for the CAP control while $\hat{q}_{2\omega}$ is always zero for the CRP control. However, $\hat{q}_{2\omega}$ is increasing towards infinity for the CAP control. This is expected since infinitely high unbalanced currents would be necessary to transfer non-zero average power without active power oscillations when the amplitudes of the positive and negative sequence voltages approach equal values (corresponding to single-phase operation). It can also be seen from Fig. 4 b) and Fig. 4 c) that the active and reactive power oscillations are significantly higher with the NSVI than with BPSC. However, the oscillating components with the NSVI are depending on the virtual impedance values, which could be selected according to how the VSM should contribute to the sharing of negative sequence loading in response to unbalanced conditions.

B. *Power transfer capability under unbalanced conditions*

A similar approach as presented for evaluating the power flow characteristics of the BPSC, CAP, RPC and NSVI control can also be applied to calculate the power transfer capability of the converter within a specific ac-side current limitation. For simplicity, a vector amplitude limitation (and not a phase current limitation that would depend on the phase angle of the negative sequence current) is considered as:

$$I_{\lim} = \left|\hat{i}_v^+\right| + \left|\hat{i}_v^-\right| = \sqrt{\hat{i}_{v,d}^{+\,2} + \hat{i}_{v,q}^{+\,2}} + \sqrt{\hat{i}_{v,d}^{-\,2} + \hat{i}_{v,q}^{-\,2}}\,. \quad (18)$$

Utilizing (4) and (15) to express the positive sequence currents and applying the expressions for the negative sequence currents from (8), (10), (12) or (14), results in an equation with only δ_{VSM} as unknown. Thus, it is possible to solve for δ_{VSM} as a function of the current limitation and the positive and negative sequence voltage amplitudes. Substituting this angle back into the expression for the average power flow results in a capability curve for the ac-side of the converter within a current limit. The resulting characteristics of the BPSC, CAP, CRP and NVSI control strategies are plotted in Fig. 5, when assuming $|\mathbf{v}_o^+| = 1.0 - |\mathbf{v}_o^-|$. Again, the coloured lines represent the different cases with accurate parameters, while the black dotted lines correspond to the results from ignoring the virtual resistances.

From the curves in Fig. 5, it is clearly seen how the power transfer capability with the CAP control approaches zero, when $|\mathbf{v}_o^-|=|\mathbf{v}_o^+|=0.5$ pu, as expected. Furthermore, the power transfer capability with the BPNC control is decreasing linearly with the positive sequence voltage amplitude, while the CRP control enables a higher power transfer capability in this case. The main reason for this higher power transfer capability of the CRP is that the negative sequence currents in this case contribute positively to the average power transfer. Finally, with the assumed parameters, the case with the NSVI has the lowest power transfer capability due to the high resulting negative sequence currents. Indeed, with the assumed value of l_{VI}^-=0.4, a negative sequence voltage amplitude of 0.4

This article has been accepted for publication in a future issue of this journal, but has not been fully edited. Content may change prior to final publication. Citation information: DOI 10.1109/JESTPE.2022.3175169, IEEE Journal of Emerging and Selected Topics in Power Electronics

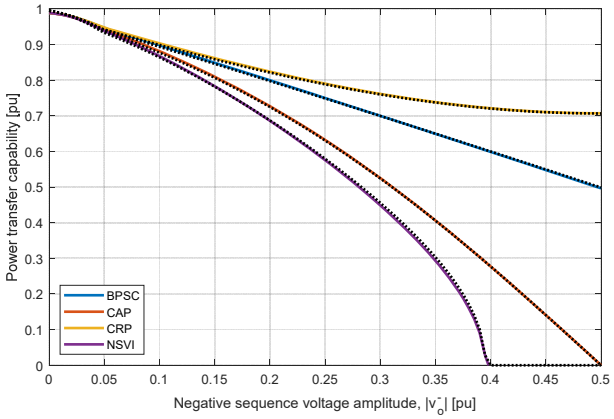

Fig. 5 Power transfer capability curve within current amplitude limitation of I_{lim} = 1.0 pu, for BPSC, CAP, CRP and NSVI control. Solid lines represent the accurate solution with the assumed parameters while dotted black lines represent the results obtained with $r_{VI}^{+} = 0$ and $r_{VI}^{-} = 0$.

pu results in approximately 1.0 negative sequence currents. This implies that there will be no remaining current capability for transferring active power, as seen in Fig. 5.

V. SIMULATION RESULTS

To assess the performance of the 5 studied strategies for control of the negative sequence currents, numerical simulations under unbalanced conditions have been conducted. A MMC has been selected as a VSC to illustrate that the functionalities of the negative sequence control approaches are generally applicable to HVDC systems and other large converter units in the transmission system. Indeed, the analysis in the previous sections is generally independent of the converter topology when only ac-side variables are studied. The simulation results are obtained with a single MMC-based terminal of an HVDC transmission system while assuming a constant dc-side voltage and include the response to an islanding event with a local load. As already mentioned, the implementation of the circulating current control and the energy balancing control indicated in Fig. 1 are documented and discussed in [36].

A. Simulation results

The parameters used for the simulations is shown in Table I, where the circuit parameters are obtained from [42]. In the following, results of different simulations are shown to highlight the response of the systems to an islanding event and to load steps in islanded mode.

1) Islanding event

A dedicated simulation has been performed to test the performance of the VSM-controlled MMC when transitioning from grid-connected to islanded mode under unbalanced conditions. For these simulations, unbalanced conditions under islanded operation are created by a balanced delta-connected load with impedances Z_L (10 pu and cos ϕ=0.99) and an additional load between phase a and b with an impedance of 0.5 Z_L. Before the islanding, the PCC is initially connected to an ideal voltage source supplying all the unbalanced currents. Fig. 6 shows the three phase voltages and

TABLE I – PARAMETERS FOR THE SIMULATION

MMC data	
Nominal power , P_{nom}	1000 MW
Nominal line-to-line grid voltage, $V_{g,nom}$	333 kV
Nominal dc side voltage, V_{DC}	640 kV
Number of modules per arm, N	400
Arm inductor, l_f	50 mH
Submodule capacitance, C_{SM}	10 mF
Transformer inductance L_T	28.2 mH
Transformer resistance R_T	0.9 Ω
Control parameters	
Frequency droop gain, k_w	20 pu
VSM damping coefficient, k_d	200 pu
Virtual inertia, T_a (=2H)	10 s
Reactive power droop gain, k_q	0 pu
Voltage limiting factor, $k_{v,\lim}$	1.05
Positive Sequence Virtual Impedance, l_{VI}^{+}, r_{VI}^{+}	0.2 pu, 0.01 pu
Negative Sequence Virtual Impedance, l_{VI}^{-}, r_{VI}^{-}	0.4 pu, 0.02 pu
PR Current Controller gains, $k_{c,P}$, $k_{c,R}$	0.8 pu, 0.3 pu
Negative Sequence Voltage Controller gains $k_{P,NS}$, $k_{i,NS}$	0.3 pu, 5 pu
Circulating Current Controller gains, $k_{cc,P}$, $k_{cc,i}$, $k_{cc,R(w)}$, $k_{cc,R(2w)}$	0.9 pu, 630 pu 0.06 pu, 0.08 pu
Sum Energy Controller gains, $k_{P,\Sigma}$, $k_{i,\Sigma}$	0.5 pu, 6 pu
Difference Energy Controller gains , $k_{P,\Delta}$, $k_{i,\Delta}$	0.6 pu, 6 pu

currents as well as the active and reactive power flow from the converter with the five different strategies for controlling the negative sequence currents as discussed in section III. At time t = 0.03 s the ideal grid voltage is disconnected, and the system starts operating in islanded mode.

From Fig. 6 a) it can be confirmed that the BPSC is injecting balanced currents even with the unbalanced load. However, this causes unbalanced voltages and corresponding power oscillations. Thus, this strategy should not be preferred for islanded operation. As shown in Fig. 6 b) and c), the CAP and CRP strategies allow for eliminating oscillations in the active and reactive power, respectively. However, this also results in unbalanced voltages and currents, although the CAP contributes to a reduction of the voltage unbalance while the CRP clearly aggravates the voltage unbalance. It should be noted that the power flow is significantly reduced for the CRP strategy, since the positive sequence voltage is limited to avoid generating over-voltages in the phase with the lowest load, as explained in II. B. As for the BPSC, the CAP and CRP strategies are not recommended for islanded operation.

The results in Fig. 6 d) show how the NSVI is significantly reducing the voltage unbalance by supplying negative sequence currents. Since there is no closed loop control on the voltages, the NSVI cannot eliminate the voltage unbalance but provides an inherent capability for sharing of negative sequence load. Finally, the results with the NSVC are shown in Fig. 6 e) and demonstrate how the closed loop control can ensure balanced voltages at the local load. However, this requires a higher negative sequence current and results in higher double frequency oscillations in the power since the unbalanced loads are supplied by the rated voltage in all phases. It should be noted that the NSVC would not be applicable in grid connected operation with a low equivalent grid impedance since negative sequence current injection from the converter would not have significant influence on the local grid voltages.

This article has been accepted for publication in a future issue of this journal, but has not been fully edited. Content may change prior to final publication. Citation information: DOI 10.1109/JESTPE.2022.3175169, IEEE Journal of Emerging and Selected Topics in Power Electronics

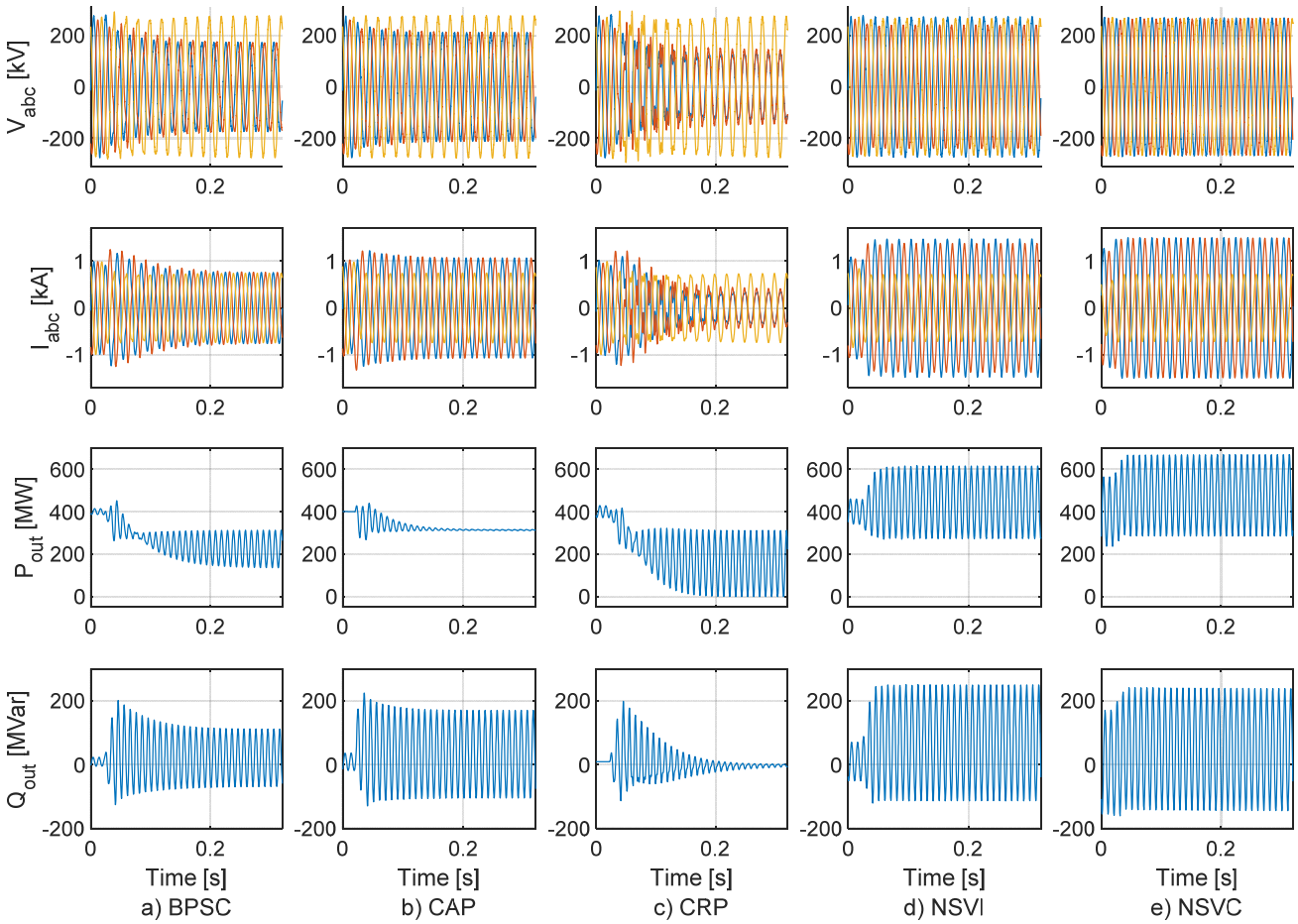

Fig. 6. Simulation of islanding event with unbalanced load and negative sequence current control by a) BPSC, b) CAP, c) CRP, d) NSVI, e) NSVC

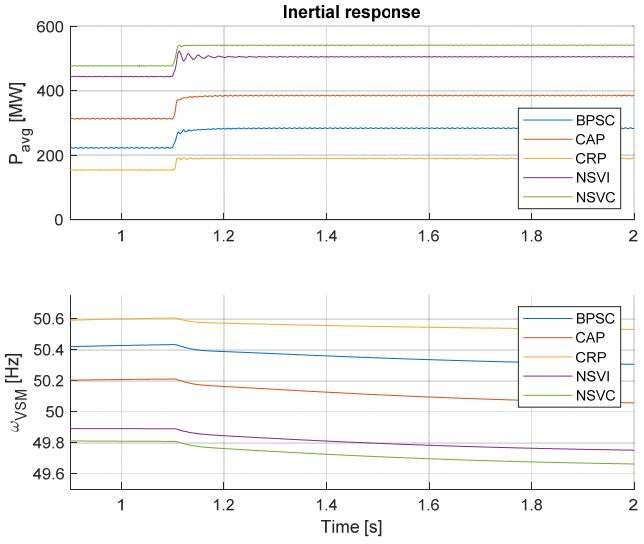

Fig. 7. Simulation results showing inertial response for load perturbation in islanded mode under unbalanced load.

2) Load step change

To test the dynamic behavior of the islanded system controlled with the different strategies, an additional impedance load, equivalent to 0.1 pu (100MW) at rated voltage, is applied at time t=1.1s. The resulting dc-component of the active power flow and the virtual speed of the VSM swing equation are shown in Fig. 7. The initial values of the active power flow and the speed are different among the different strategies since they depend on the response of the control strategy to the islanding event from Fig. 6. However, the step in the power absorbed by the load and the resulting inertial response of the VSM speed can be clearly seen for all the different strategies. This demonstrates how the grid forming control relying on the virtual swing equation retains the intended operation independently of how the unbalances in the isolated system are managed.

VI. EXPERIMENTAL VERIFICATION

The operation of the proposed VSM-implementation and the performance of the five different strategies for negative sequence current control under unbalanced conditions has been verified in grid connected mode by experimental results with a small-scale laboratory setup.

A. Experimental setup

The experimental setup consists of a 50 kW MMC prototype designed for operation with ac-side line voltages up to 400 V RMS. The MMC prototype has 12 half bridge

TABLE II – PARAMETERS OF EXPERIMENTAL SETUP

Rated power	50 kVA
Rated line-to-line grid voltage	400 V
Rated dc voltage	700 V
Number of modules per arm	12
Module capacitance	15 mF
Arm inductance	1.4 mH
Control time-step	80 us

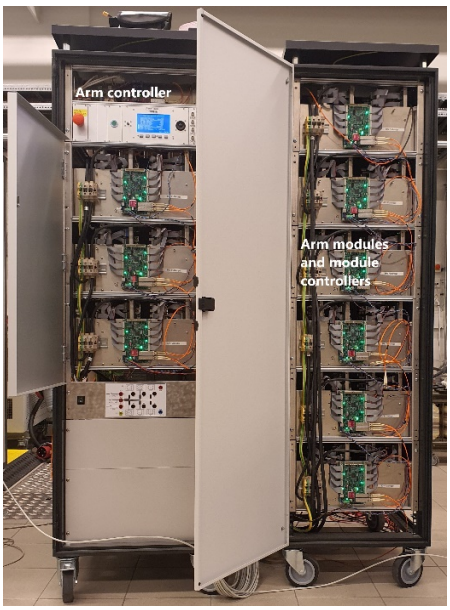

Fig. 8. Photo of MMC used in the experimental setup

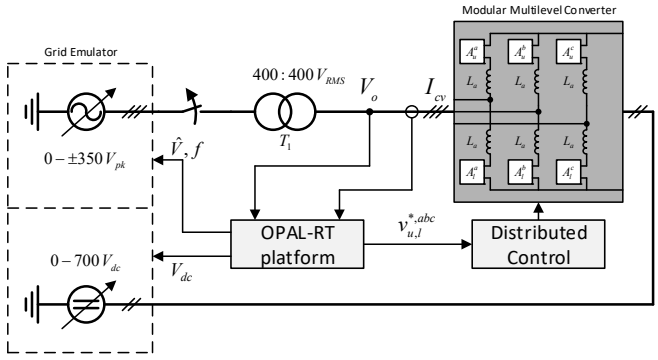

Fig. 9. Schematic overview of experimental setup

modules per arm and the most relevant characteristics are summarized in Table II. A picture of the converter setup with indication of the main elements is shown in Fig. 8. The local control of each arm is implemented on a PicoZed mezzanine board containing a Zynq 7030 chip by Xilinx and includes functions for the arm balancing and modulation, as indicated in Fig. 1. The balancing of the modules within one arm is obtained by means of a sorting algorithm according to [33], while the modulation technique is the phase-disposition PWM (PDPWM) applying the PWM signal only to one module per arm at a time. Further details on the distributed control of the modules in each arm are provided in [32]. The insertion indices for each arm are calculated from the voltage references V_v^* and V_{cir}^* according to [34].

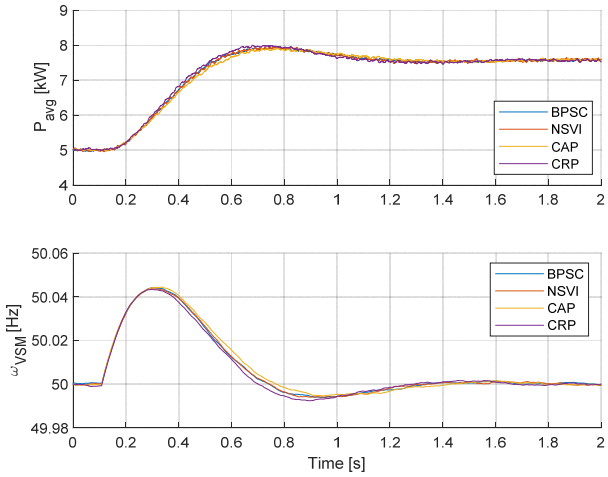

Fig. 10. Experimental results showing response to change of power reference under unbalanced conditions

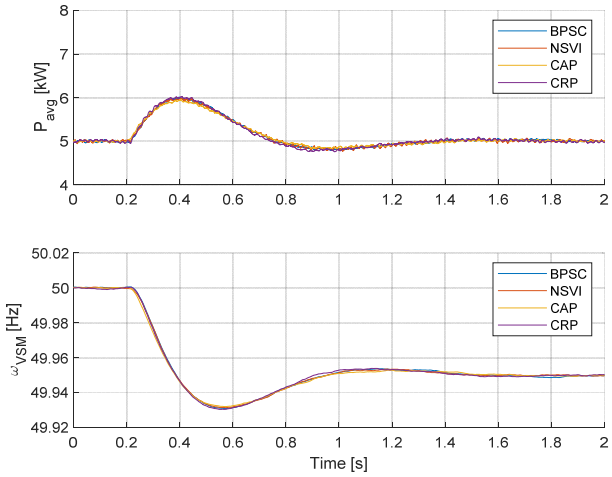

Fig. 11. Experimental results showing response to frequency perturbation under unbalanced conditions

The voltage references for each arm of the MMC are provided by an OPAL-RT platform used to implements all the remaining control features. Furthermore, an EGSTON COMPISO switch-mode amplifier is used as a grid emulator to impose perturbations in the ac-side of the MMC. Two available channels from the same amplifier are also providing the dc voltage to the MMC prototype. A schematic overview of the experimental setup is shown in Fig. 9.

B. Verification of inertial response to power and frequency perturbation under unbalanced conditions

A complete set of experiments has been conducted to verify the performance of the different methods for generating the negative sequence current references. The tests are performed with a 25% voltage unbalance imposed by the grid emulator.

First, the transient response of the VSM-based control system has been tested for a variation of the power reference and with a disturbance in the grid frequency under the unbalanced conditions. The response to a step of the power

This article has been accepted for publication in a future issue of this journal, but has not been fully edited. Content may change prior to final publication. Citation information: DOI 10.1109/JESTPE.2022.3175169, IEEE Journal of Emerging and Selected Topics in Power Electronics

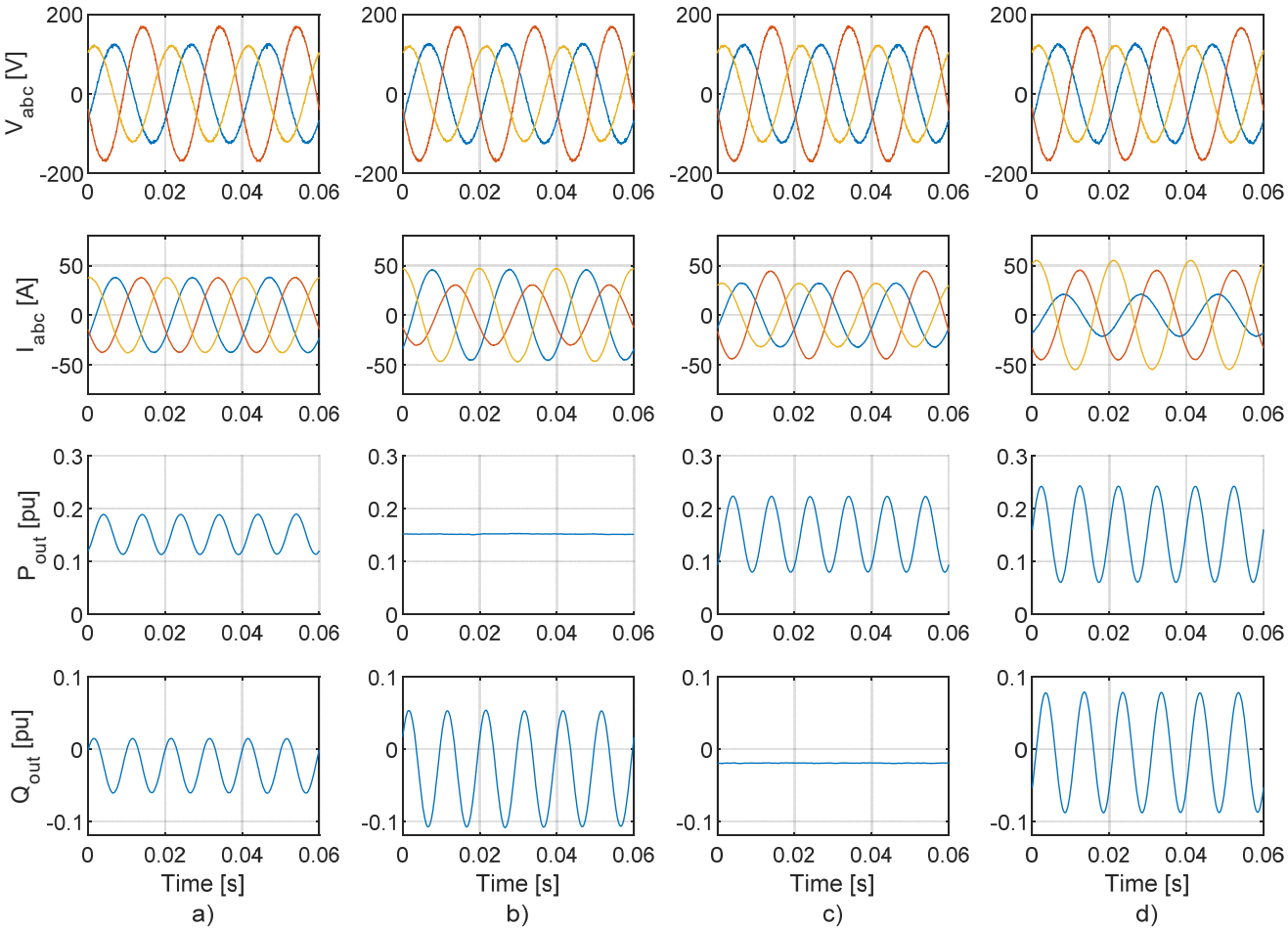

Fig. 12. Experimental results demonstrating VSM-based operation under unbalanced conditions with a) BPSC, b) CAP, c) CRP, d) NSVI

reference from 5 kW to 7.5 kW is shown in Fig. 10. The transients in the average power according to (1) and the virtual speed of the swing equation highlights the inertial behavior of the VSM control. Moreover, the effect of the negative sequence currents is marginal and the four control strategies provide almost identical responses.

The response to a perturbation in the grid frequency imposed as a step from 1 pu to 0.999 pu (i.e., from 50 Hz to 49.95 Hz) in the frequency imposed by the grid emulator is shown in Fig. 11. This frequency disturbance triggers the reaction of the virtual inertia, and the converter reacts with an increase in the power transfer. The rotating speed of the virtual inertia follows a similar transient and settles at the new grid frequency after a well damped inertial response. The effect of the negative sequence control is again negligible.

C. *Verification of negative sequence current control under unbalanced conditions*

Experimental results at steady state conditions for four different strategies for controlling the negative sequence currents (i.e. BPSC, CAP, CRP, NSVI) are shown in Fig. 12. The results clearly indicate that the control objectives are fulfilled, and that the converter operates as expected. Indeed, the output currents exhibit unbalances except for the BPSC where only the positive sequence is present. It is also clear how the oscillations in active or the reactive power flow are eliminated with the CAP and the CRP strategies, respectively. The amplitudes of the power oscillations also correspond to the analytical evaluation from section II. The case with the NSVI shows a negative sequence component proportional to the imposed negative sequence voltage. The NSVC strategy is not tested since the system is operated in grid connected mode with negligible grid impedance beyond the transformer. Thus, the NSVC would not be applicable since the ac-side voltages cannot be balanced by negative sequence current injection from the MMC.

VII. GENERAL CHARACTERISTICS AND APPLICABILITY OF EVALUATED STRATEGIES FOR NEGATIVE SEQUENCE CURRENT CONTROL

To provide a comparative assessment of the different investigated strategies for controlling the negative sequence current components of a VSM, the general characteristics and the experiences from the simulations and laboratory testing are summarized in Table III. The entries of the table highlight how the three strategies for calculating the negative sequence

TABLE III – COMPARISON OF CHARACTERISTICS AND APPLICABILITY OF DIFFERENT VSM-BASED STRATEGIES FOR NEGATIVE SEQUENCE CURRENT CONTROL

Control Strategy	General characteristics and applicability under unbalanced conditions		
	Grid connected in strong grid	**Grid-connected in weak grid**	**Islanded**
BPSC	• Balanced three phase currents • Active and Reactive power oscillations Suitable for: **Maintaining balanced currents in all conditions**	Same as for strong grids	• Maintains balanced currents without supporting unbalanced loads • Worsens voltage unbalance **Not practically relevant**
CAP	• Unbalanced currents with highest current in the phase with lowest voltage • Eliminated active power oscillations and high reactive power oscillations • Not applicable for severe unbalanced faults with zero remaining voltage in faulted phase Suitable for: **transferring constant active power to the PCC under moderate unbalances**	Same as for strong grids, with the following additional implications: • Reduces voltage unbalance when injecting power • Worsens voltage unbalance when consuming power	• Attempts to control active power without considering voltage unbalance • Can reduce voltage unbalance when injecting power depending on load characteristics **Not practically relevant**
CRP	• Unbalanced currents with phase current amplitude proportional to the phase voltage amplitude • Eliminated reactive power oscillations and high active power oscillations Suitable for: **Maximum power transfer to the PCC**	Same as for strong grids	• Attempts to control reactive power without considering voltage unbalance • Will imply highest currents in the phase with the highest voltage, and significantly worsened unbalance **Not applicable**
NSVI	• Negative sequence current proportional to negative sequence voltage Suitable for: **Handling large variations in operating conditions and grid impedance**	Same as for strong grid, with additional advantage of: • Impedance-based contribution to sharing of unbalanced loading in the grid • Inherently suitable for parallel operation with other similar units	• Impedance-based sharing of unbalanced loading in the grid • Attenuates but cannot eliminate voltage unbalances Suitable for: **Handling large variations in operating conditions and load impedance**
NSVC	• Controller will saturate when negative sequence current cannot influence the local voltage unbalance **Not applicable**	• Provides unbalanced currents to balance the local voltage • Can eliminate local voltage unbalances if the equivalent grid impedance is large • Not inherently robust for large variations in grid impedance Suitable for: **Eliminating local voltage unbalances when grid impedance will always be high**	• Can eliminate local voltage unbalances for all loadings within the converter rating • Parallel operation of multiple units will require droop-based control or other mechanisms for load sharing Suitable for: **Providing balanced voltages in islanded systems with unbalanced loads**

current references to shape the power flow characteristics, i.e., the BPSC, CAP and CRP, are suitable for grid connected operation, but not directly applicable in islanded conditions. However, the CAP strategy is only applicable for limited unbalances, as elimination of power oscillations will not be possible for severe unbalances when the three-phase grid is approaching single-phase operation. Similarly, the NSVC is most relevant for islanded systems, and unapplicable for grid connected operation in strong grids, even if it can be relevant for operation in very weak grid conditions when the local voltage unbalance can be regulated by the converter. The NSVI is generally applicable in all operating conditions, but in strong grid condition this strategy can result in high negative sequence currents without fulfilling any specific objective for the converter operation.

The presented results and discussions show that there is no single strategy that will be most suitable for all conditions. This implies that further attention should be dedicated to the optimal selection of the negative sequence current control strategy under changing operating conditions, or during changes between grid-connected and islanded operation.

VIII. CONCLUSIONS

This paper presents a detailed assessment and comparative evaluation of virtual synchronous machine-based control strategies designed for operating under unbalanced grid conditions. Five different alternatives for controlling the negative sequence currents have been considered and compared, theoretically, by simulation, and by experimental validation with a Modular Multilevel Converter. The strategies for controlling the negative sequence currents define the response to grid voltage unbalances or load unbalances and include control objectives for obtaining: i) Balanced three phase currents, ii) elimination of second harmonic oscillations in the active power flow, iii) elimination of second harmonic oscillations in the reactive power flow, iv) a negative sequence virtual impedance for sharing of negative sequence loading between the VSM and the rest of the grid or v) closed loop control for elimination of negative sequence components in the local ac voltage. The applicability of these strategies when connected to a strong grid, a weak grid with high equivalent impedance or a stand-alone system with local loads have also been discussed. Results from theoretical analysis, numerical simulations and experimental testing demonstrate how the

presented control strategy can fulfill the selected control objectives. The power flow characteristics and the power transfer capability with the different strategies have also been analyzed. Further work related to the presented control methods will be focused on development of coordinated strategies for limitation of the current references and for maintaining the grid-forming functionality of the VSM-based control in case of severe fault conditions.

APPENDIX A: SIMPLIFIED ANALYTICAL EXPRESSIONS FOR POWER FLOW COMPONENTS UNDER UNBALANCED CONDITIONS

The analytical expression resulting from further evaluation of the different strategies for negative sequence current control in section III. are presented in the following.

A. Balanced Positive Sequence Current (BPSC) control

Setting r_{VI}^{+}=0 in (16), and simplifying the expressions by defining the virtual reactance as $x_{VI}^{+}=\omega_{VSM}\, l_{VI}^{+}$, the equation can be easily solved for δ_{VSM}, as given by

$$\delta_{vsm}=\sin^{-1}\left(\frac{x_{VI}^{+}p_o^{*}}{\hat{v}_e^{+*}\left|\mathbf{v}_o^{+}\right|}\right). \tag{19}$$

Thus, the average reactive power flow under the assumption of r_{VI}^{+}=0.01 can be expressed as

$$\bar{q}_o=\frac{\sqrt{\left(\left|\mathbf{v}_o^{+}\right|\hat{v}_e^{+*}\right)^2-\left(x_{VI}^{+}p_o^{*}\right)^2}-\left|\mathbf{v}_o^{+}\right|^2}{x_{VI}^{+}}. \tag{20}$$

Finally, an expression for the amplitude of the active and reactive power oscillations can be obtained as:

$$\hat{p}_{2\omega}=\hat{q}_{2\omega}=\frac{\hat{v}_o^{-}}{x_{VI}^{+}}\sqrt{\left(\hat{v}_e^{+*}\right)^2+\left|\mathbf{v}_o^{+}\right|^2-2\sqrt{\left(\hat{v}_e^{+*}\left|\mathbf{v}_o^{+}\right|\right)^2-\left(x_{VI}^{+}p_o^{*}\right)^2}}. \tag{21}$$

B. Constant Active Power (CAP) control

The detailed expressions for the average active and reactive power flow in this case can be obtained as:

$$\bar{p}_o=\frac{\left|\mathbf{v}_o^{+}\right|^2-\left|\mathbf{v}_o^{-}\right|^2}{\left|\mathbf{v}_o^{+}\right|}\cdot\frac{x_{VI}^{+}\hat{v}_e^{+*}\sin\delta_{VSM}+r_{VI}^{+}\hat{v}_e^{+*}\cos\delta_{VSM}-r_{VI}^{+}\left|\mathbf{v}_o^{+}\right|}{\left(r_{VI}^{+}\right)^2+\left(x_{VI}^{+}\right)^2} \tag{22}$$

$$\bar{q}_o=\frac{\left|\mathbf{v}_o^{+}\right|^2+\left|\mathbf{v}_o^{-}\right|^2}{\left|\mathbf{v}_o^{+}\right|}\cdot\frac{x_{VI}^{+}\hat{v}_e^{+*}\cos\delta_{VSM}-x_{VI}^{+}\left|\mathbf{v}_o^{+}\right|-r_{VI}^{+}\hat{v}_e^{+*}\sin\delta_{VSM}}{\left(r_{VI}^{+}\right)^2+\left(x_{VI}^{+}\right)^2}. \tag{23}$$

Setting r_{VI}^{+}=0 in (22) and solving for δ_{VSM} when assuming the average active power flow to be equal to the reference results in:

$$\delta_{vsm}=\sin^{-1}\left(\frac{x_{VI}^{+}\cdot\left|\mathbf{v}_o^{+}\right|}{\hat{v}_e^{+*}\left(\left|\mathbf{v}_o^{+}\right|^2-\left|\mathbf{v}_o^{-}\right|^2\right)}p_o^{*}\right). \tag{24}$$

Thus, the average reactive power flow can be expressed as:

$$\bar{q}_o=\frac{\left(\left|\mathbf{v}_o^{+}\right|^2+\left|\mathbf{v}_o^{-}\right|^2\right)}{x_{VI}^{+}}\left(\sqrt{\left(\frac{\hat{v}_e^{+*}}{\left|\mathbf{v}_o^{+}\right|}\right)^2+\left(\frac{x_{VI}^{+}p_o^{*}}{\left|\mathbf{v}_o^{+}\right|^2-\left|\mathbf{v}_o^{-}\right|^2}\right)^2}-1\right). \tag{25}$$

While the double frequency active power oscillations in this case are controlled to zero, the amplitude of the reactive power oscillations can be calculated as:

$$\hat{q}_{2\omega}=\frac{2\left|\mathbf{v}_o^{-}\right|}{x_{VI}^{+}}\sqrt{\left(\hat{v}_e^{+*}\right)^2+\left|\mathbf{v}_o^{+}\right|^2-2\hat{v}_e^{+*}\left|\mathbf{v}_o^{+}\right|}\sqrt{1-\left(\frac{x_{VI}^{+}\left|\mathbf{v}_o^{+}\right|p_o^{*}}{\hat{v}_e^{+*}\left(\left|\mathbf{v}_o^{+}\right|^2-\left|\mathbf{v}_o^{-}\right|^2\right)}\right)^2}. \tag{26}$$

C. Constant Reactive Power (CRP) control

The detailed expressions for the average active and reactive power flow in this case can be obtained as

$$\bar{p}_o=\frac{\left|\mathbf{v}_o^{+}\right|^2+\left|\mathbf{v}_o^{-}\right|^2}{\left|\mathbf{v}_o^{+}\right|}\cdot\frac{x_{VI}^{+}\hat{v}_e^{+*}\sin\delta_{VSM}+r_{VI}^{+}\hat{v}_e^{+*}\cos\delta_{VSM}-r_{VI}^{+}\left|\mathbf{v}_o^{+}\right|}{\left(r_{VI}^{+}\right)^2+\left(x_{VI}^{+}\right)^2} \tag{27}$$

$$\bar{q}_o=\frac{\left(\left|\mathbf{v}_o^{+}\right|^2-\left|\mathbf{v}_o^{-}\right|^2\right)}{\left|\mathbf{v}_o^{+}\right|}\cdot\frac{x_{VI}^{+}\left|\mathbf{v}_o^{+}\right|+r_{VI}^{+}\hat{v}_e^{+*}\sin\delta_{VSM}-x_{VI}^{+}\hat{v}_e^{+*}\cos\delta_{VSM}}{\left(r_{VI}^{+}\right)^2+\left(x_{VI}^{+}\right)^2}. \tag{28}$$

Setting r_{VI}^{+}= 0 in (27) and solving for δ_{VSM} results in

$$\delta_{vsm}=\sin^{-1}\left(\frac{x_{VI}^{+}\cdot\left|\mathbf{v}_o^{+}\right|p_o^{*}}{\hat{v}_e^{*}\left(\left|\mathbf{v}_o^{+}\right|^2+\left|\mathbf{v}_o^{-}\right|^2\right)}\right). \tag{29}$$

The expression for the average reactive power can then be simplified to

$$\bar{q}_o=\frac{\left(\left|\mathbf{v}_o^{+}\right|^2-\left|\mathbf{v}_o^{-}\right|^2\right)}{x_{VI}^{+}}\left(1-\sqrt{\left(\frac{\hat{v}_e^{+*}}{\left|\mathbf{v}_o^{+}\right|}\right)^2-\left(\frac{x_{VI}^{+}p_o^{*}}{\left|\mathbf{v}_o^{+}\right|^2+\left|\mathbf{v}_o^{-}\right|^2}\right)^2}\right). \tag{30}$$

While the double frequency reactive power oscillations in this case are controlled to zero, the amplitude of the active power oscillations can be calculated as

$$\hat{p}_{2\omega}{}^{2}=\frac{2\left|\mathbf{v}_o^{-}\right|}{x_{VI}^{+}}\sqrt{\left(\hat{v}_e^{+*}\right)^2+\left|\mathbf{v}_o^{+}\right|^2-2\hat{v}_e^{+*}\left|\mathbf{v}_o^{+}\right|}\sqrt{1-\left(\frac{x_{VI}^{+}\left|\mathbf{v}_o^{+}\right|p_o^{*}}{\hat{v}_e^{+*}\left(\left|\mathbf{v}_o^{+}\right|^2+\left|\mathbf{v}_o^{-}\right|^2\right)}\right)^2}. \tag{31}$$

D. Negative Sequence Virtual Impedance (NSVI) control

By defining $x_{VI}^{-}=\omega_{VSM}\, l_{VI}^{-}$, the detailed expressions for the average active and reactive power flow with the NSVI control are given by (32) and (33), respectively. However, if the negative sequence virtual resistance r_{VI}^{+}= 0, the negative sequence currents will not transfer average active power. Thus, only the positive sequence components will contribute to the average power transfer and the power balance reduces to the same expression as for the BPSC control. Thus, utilizing (19), the magnitude of the power components can be derived analytically as for the other cases. The resulting average

$$\bar{p}_o = \frac{\hat{v}_e^{+*}\left|\mathbf{v}_o^+\right|\left(x_{VI}^+\sin\delta_{VSM}+r_{VI}^+\cos\delta_{VSM}\right)\left(\left(r_{VI}^-\right)^2+\left(x_{VI}^-\right)^2\right)-r_{VI}^+\left(x_{VI}^-\right)^2\left|\mathbf{v}_o^+\right|^2-r_{VI}^-\left(x_{VI}^+\right)^2\left|\mathbf{v}_o^+\right|^2-r_{VI}^+\left(r_{VI}^-\right)^2\left|\mathbf{v}_o^+\right|^2-r_{VI}^-\left(r_{VI}^+\right)^2\left|\mathbf{v}_o^-\right|^2}{\left(\left(r_{VI}^+\right)^2+\left(x_{VI}^+\right)^2\right)\left(\left(r_{VI}^-\right)^2+\left(x_{VI}^-\right)^2\right)} \tag{32}$$

$$\bar{q}_o = \frac{\left(x_{VI}^+\hat{v}_e^{+*}\left|\mathbf{v}_o^+\right|\cos\delta_{VSM}-r_{VI}^+\hat{v}_e^{+*}\left|\mathbf{v}_o^+\right|\sin\delta_{VSM}-x_{VI}^+\left|\mathbf{v}_o^+\right|^2\right)\left(\left(r_{VI}^-\right)^2+\left(x_{VI}^-\right)^2\right)-x_{VI}^-\left|\mathbf{v}_o^-\right|^2\left(\left(x_{VI}^+\right)^2+\left(r_{VI}^+\right)^2\right)}{\left(\left(r_{VI}^+\right)^2+\left(x_{VI}^+\right)^2\right)\left(\left(r_{VI}^-\right)^2+\left(x_{VI}^-\right)^2\right)} \tag{33}$$

$$\hat{p}_{2\omega} = \frac{\left|\mathbf{v}_o^-\right|}{x_{VI}^+x_{VI}^-}\sqrt{\left(x_{VI}^+\right)^2\left|\mathbf{v}_o^+\right|^2+\left(x_{VI}^-\right)^2\left(\left|\mathbf{v}_o^+\right|^2+\left(\hat{v}_e^{+*}\right)^2-2\hat{v}_e^{+*}\left|\mathbf{v}_o^+\right|\sqrt{1-\left(\frac{x_{VI}^+p_o^*}{\hat{v}_e^{+*}\left|\mathbf{v}_o^+\right|}\right)^2}\right)+2x_{VI}^+x_{VI}^-\left|\mathbf{v}_o^+\right|\left(\hat{v}_e^{+*}\sqrt{1-\left(\frac{x_{VI}^+p_o^*}{\hat{v}_e^{+*}\left|\mathbf{v}_o^+\right|}\right)^2}-\left|\mathbf{v}_o^+\right|\right)}} \tag{32}$$

$$\hat{q}_{2\omega} = \frac{\left|\mathbf{v}_o^-\right|}{x_{VI}^+x_{VI}^-}\sqrt{\left(x_{VI}^+\right)^2\left|\mathbf{v}_o^+\right|^2+\left(x_{VI}^-\right)^2\left(\left|\mathbf{v}_o^+\right|^2+\left(\hat{v}_e^{+*}\right)^2-2\hat{v}_e^{+*}\left|\mathbf{v}_o^+\right|\sqrt{1-\left(\frac{x_{VI}^+p_o^*}{\hat{v}_e^{+*}\left|\mathbf{v}_o^+\right|}\right)^2}\right)-2x_{VI}^+x_{VI}^-\left|\mathbf{v}_o^+\right|\left(\hat{v}_e^{+*}\sqrt{1-\left(\frac{x_{VI}^+p_o^*}{\hat{v}_e^{+*}\left|\mathbf{v}_o^+\right|}\right)^2}-\left|\mathbf{v}_o^+\right|\right)}} \tag{33}$$

reactive power flow is given by

$$\bar{q}_o = \frac{x_{VI}^-\hat{v}_e^{+*}\left|\mathbf{v}_o^+\right|\sqrt{1-\left(\frac{x_{VI}^+p_o^*}{\hat{v}_e^{+*}\left|\mathbf{v}_o^+\right|}\right)^2}-x_{VI}^-\left|\mathbf{v}_o^+\right|^2-x_{VI}^+\left|\mathbf{v}_o^-\right|^2}{x_{VI}^+x_{VI}^-}, \tag{34}$$

and the amplitudes of the double frequency oscillations in active and reactive power are given by (35) and (36), respectively.

REFERENCES

[1] S. C. Johnson, J. D. Rhodes, M. E. Webber, "Understanding the impact of non-synchronous wind and solar generation on grid stability and identifying mitigation pathways," in *Applied Energy*, Vol. 262, ID 114492, 11 pp., March 2020

[2] J. O'Sullivan, A. Rogers, D. Flynn, P. Smith, A. Mullane, M. O'Malley, "Studying the Maximum Instantaneous Non-Synchronous Generation in an Island System – Frequency Stability Challenges in Ireland," in *IEEE Transactions on Power Systems*, Vol. 29, No. 6, pp. 2943-2951, November 2014

[3] M. Yu, A. Dysko, C. Booth, A. Roscoe, J. Zhu, H. Urdal, "Investigations of the constraints relating to penetration of non-synchronous generation (NSG) in future power systems," in *Proceedings of the Sixth Protection, Automation and Control World Conference*, PAC World, 29 June – 2 July 2015, 9 pp.

[4] M. Yu, A. J. Roscoe, A. Dyśko, C. D. Booth, R. Ierna, J. Zhu, H. Urdal, "Instantaneous penetration level limits of non-synchronous devices in the British power system," in *IET Renewable Power Generation* Vol. 11, No. 8, pp. 1211-1217, June 2017.

[5] J. Rocabert, A. Luna, F. Blaabjerg, P. Rodriguez, "Control of power converters in AC microgrids. IEEE transactions on power electronics, Vol. 27, No. 11, pp. 4734-4749, November 2012

[6] R. Rosso, X. Wang, M. Liserre, X. Lu, S. Engelken, "Grid-Forming Converters: Control Approaches, Grid-Synchronization, and Future Trends—A Review," in *IEEE Open Journal of Industry Applications*, Vol. 2, pp. 93-109, April 2021

[7] ENTSO-E Technical Group on High Penetration of Power Electronic Interfaced Power Sources, Tehcnial Report "High Penetration of Power Electronic Interfaced Power Sources and the Potential Contribution of Grid Forming Converters, 2020, available from: https://euagenda.eu/upload/publications/untitled-292051-ea.pdf

[8] ENTSO-E, "Grid-Forming Capabilities:Towards System Level Integration", March 2021, available from: https://eepublicdownloads.entsoe.eu/clean-documents/RDC%20documents/210331_Grid%20Forming%20Capabilities.pdf

[9] National Grid, Grid Code Working Group GC037, "Minimum Specification Required for Provision of GB Grid Forming (GBGF) Capability (formerly Virtual Synchronous Machine/VSM Capability)", https://www.nationalgrideso.com/industry-information/codes/grid-code-old/modifications/gc0137-minimum-specification-required

[10] AEMO White Paper, August 2021, "Application of Advanced Grid-scale Inverters in the NEM," available from https://aemo.com.au/-/media/files/initiatives/engineering-framework/2021/application-of-advanced-grid-scale-inverters-in-the-nem.pdf?la=en&hash=B4E20D68B23F66090ADA5FD47A50D904

[11] ENTSO-E Technical Paper, "HVDC Links in System Operations," December 2019, available from https://eepublicdownloads.entsoe.eu/clean-documents/SOC%20documents/20191203_HVDC%20links%20in%20system%20operations.pdf

[12] J. Zhu, C. D. Booth, G. P. Adam, A. J. Roscoe, C. G. Bright, "Inertia Emulation Control Strategy for VSC-HVDC Transmission Systems," in *IEEE Transactions on Power Systems*, Vol. 28, No. 2, pp. 1277-1287, May 2013

[13] R. Aouini, B. Marinescu, K. B. Kilani, M. Elleuch, "Synchronverter-Based Emulation and Control of HVDC Transmission," in *IEEE Transactions on Power Systems*, Vol. 31, No. 1, pp. 278-286, January 2016

[14] E. Rakhshani, D. Remon, A. M. Cantarellas, J. M. Garcia, P. Rodriguez, "Virtual Synchronous Power Strategy for Multiple HVDC Interonnections of Multi-Area AGC Power Systems," in *IEEE Transactions on Power Systems*, Vol. 32, No. 3, pp. 1665- 1677, May 2017

[15] H.-P. Beck, R. Hesse, "Virtual Synchronous Machine," in *Proc. of the 9th Int. Conf. on Electrical Power Quality and Utilisation*, Barcelona, Spain, 9-11 Oct. 2007, 6 pp.

[16] Q.-C. Zhong and G. Weiss, "Synchronverters: Inverters that mimic synchronous generators," *IEEE Transactions on Industrial Electronics,* Vol. 58, No. 4, pp. 1259–1267, April 2011

[17] K. Sakimoto, Y. Miura, T. Ise, "Stabilization of a power system with a distributed generator by a virtual synchronous generator function," in *Proceedings of the 8th Int. Conf. on Power Electron. – ECCE Asia*, Jeju, Korea, 30 May- 3 Jun. 2011, 8 pp.

[18] P. Rodriguez, I. Candela, A. Luna, "Control of PV Generation Systems using the Synchronous Power Controller," in *Proceedings. of the 2013 IEEE Energy Conversion Congress and Expo.*, ECCE 2013, Denver, Colorado, USA, 15-19 Sept. 2013, pp. 993-998

[19] M. Guan, W. Pan, J. Zhang, Q. Hao, J. Cheng, X. Zheng, "Synchronous Generator Emulation Control Strategy for Voltage Source (VSC)

Stations," in *IEEE Transactions on Power Systems*, Vol. 30, No. 6, pp. 3093-3101, November 2015

[20] S. D'Arco, J. A. Suul, "Virtual Synchronous Machines – Classification of Implementations and Analysis of Equivalence to Droop Controllers for Microgrids," in *Proceedings of IEEE PES PowerTech 2013*, Grenoble, France, 16-20 June 2013, 7 pp.

[21] X. Zheng, C. Wang, S. Pang, "Injecting positive-sequence current virtual synchronous generator control under unbalanced grid," in *IET Ren, Power Gen.*, Vol. 13, No. 1, pp. 165-170, Jan. 2019

[22] M. Chen, X. Xiao, Ch. Y, Sh. Tao, "Flexible Power Control of Virtual Synchronous Generators Under Unbalanced Grid Voltage Conditions," in *Proceedings of the 2017 IEEE Energy Conversion Congress and Exposition*, ECCE 2017, Cincinnati, Ohio, USA, 1-5 October 2017, pp 2881-2888

[23] T. Zheng, L. Chen, Y. Guo, S. Mei, "Flexible unbalanced control with peak current limitation for virtual synchronous generator under voltage sags" in *Journal of Modern Power Systems and Clean Energy*, Vol. 6, No. 1, pp. 61-72, January 2018

[24] T. Zheng, L. Chen, Y. Guo, Sh. Mei, "Comprehensive control strategy of virtual synchronous generator under unbalanced voltage conditions", *IET Generation, Transmission & Distribution,* Vol. 12, No. 7, pp. 1621-1630, April 2018

[25] F. Li, G. Liu, K. Zhu, W. Wang, "An Improved Control Strategy of Virtual Synchronous Generator under Unbalanced Conditions", in *Proceedings of the 2018 IEEE 4th Southern Power Electronics Conference*, SPEC 2018, Singapore, 10-13 December 2018, 6 pp.

[26] L. Shang, J. Hu, X. Yuan, Y. Huang, "Improved virtual synchronous control for grid-connected VSCs under grid voltage unbalanced conditions," in *Journal of Modern Power Systems and Clean Energy*, Vol. 7, No. 1, January 2019, pp. 174-185

[27] H. Miao, F. Mei, Y. Yang, H. Chen, J. Zheng, "A Comprehensive VSM Control Strategy Designed for Unbalanced Grids", *Energies*, Vol. 12, No. 6, March 2019, 17 pp.

[28] S. Wang, L. Han, K. Chen, "Comprehensive Coordinated Control Strategy of Virtual Synchronous Generators under Unbalanced Power Grids" in *Journal of Power Electronics*, Vol. 19, No. 6, November 2019, pp. 1554-1565

[29] W. Zhang, J. Rocabert, J. I. Candela, P. Rodriguez, "Synchronous power control of grid-connected power converters under asymmetrical grid fault," in *Energies*, Vol. 10, No. 7, 2017, 21 pp.

[30] X. Wu, J. Mei, B. Wang, D. Liang, Ch. Qin, J. Zong, "Unbalanced Loads Control Strategy for Virtual Synchronous Generator in Passive Network," in *Proceedings of the 2019 IEEE Innovative Smart Grid Technologies Conference – Asia*, ISGT-Asia 2019, Chengdu, China, 21-24 May 2019, pp. 2063-2068

[31] E. Avdiaj, J. Are Suul, S. D'Arco, L. Piegari, "A Current Controlled Virtual Synchronous Machine Adapted for Operation under Unbalanced Conditions," *9th International Conference on Renewable Energy Research and Application*, ICRERA 2020, Glasgow, UK / Virtual Conference, 27-30 September 2020, pp. 263-270

[32] S. D'Arco, G. Guidi, J. A. Suul, "Operation of a Modular Multilevel Converter Controlled as a Virtual Synchronous Machine," in *Proceedings of the International Power Electronics Conference*, IPEC 2018 ECCE Asia, Niigata, Japan, 20-24 May 2018, 8 pp.

[33] A. Lesnicar, R. Marquart, "An Innovative Modular Multilevel Converter Topology Suitable for a Wide Power Range," *in Proceedings of the 2003 IEEE Bologna PowerTech*, 23-26 June 2003, Bologna, Italy, pp. 272-277

[34] A. Antonopoulos, L. Ängquist, H.-P. Nee, "On dynamics and voltage control of the modular multilevel converter," in *Proc. of the 13th European Conference on Power Electronics and Applications*, EPE'09, Barcelona, Spain, 8-10 September 2009, 10 pp.

[35] G. Guidi, S. D'Arco, K. Nishikawa, J. A. Suul, "Load Balancing of a Modular Multilevel Grid Interface Converter for Transformer-Less Large-Scale Wireless Electric Vehicle Charging Infrastructure," in *IEEE Journal of Emerging and Selected Topics in Power Electronics*, Vol. 9, No, 4, pp. 4587-4605, August 2021

[36] E. Avdiaj, J. A. Suul, S. D'Arco, L. Piegari, "Adaptive Filtering for Energy Control of a Modular Multilevel Converter Operated as a Virtual Synchronous Machine Under Unbalanced Conditions" submitted to the *16th International Conference on Compatibility, Power Electronics and Power Engineering*, IEEE CPE-POWERENG, Birmingham, UK, 29 June – 1 July 2022, 8 pp.

[37] P. Rodriguez, A. Luna, R. S. Muñoz-Aguilar, I. Etxeberria-Otadui, R. Teodorescu, F. Blaabjerg, "A Stationary Reference Frame Grid Synchronization System for Three-Phase Grid-Connected Power Converters Under Adverse Grid Conditions", in *IEEE Transactions on Power Electronics*, Vol. 27, No. 1, pp. 99-112, January 2012

[38] P. Rodriguez A.V. Timbus, R. Teodorescu, M. Liserre, F. Blaabjerg, "Flexible Active Power Control of Distributed Power Generation Systems During Grid Faults", in *IEEE Transactions on Industrial Electronics*, Vol. 54, No. 5, pp.2583-2592, October 2007

[39] O. Mo, S. D'Arco, J. A. Suul, "Evaluation of Virtual Synchronous Machines with Dynamic or Quasi-stationary Machine Models," in *IEEE Transactions on Industrial Electronics*, Vol. 64, No. 7, pp. 5952-5962, July 2017

[40] S. D'Arco, J. A. Suul, O. B. Fosso, "A Virtual Synchronous Machine Implementation for Distributed Control of Power Converters in SmartGrids," in *Electric Power System Research*, Vol. 122, May 2015, pp. 180-197

[41] E. Avdiaj, J. A. Suul, S. D'Arco, L. Piegari, "A Virtual Synchronous Machine-based Control for Eliminating DC-side Power Oscillations of Three-Phase VSCs under Unbalanced Grid Voltages," in *Proceedings of the 2021 IEEE 15th International Conference on Compatibility, Power Electronics and Power Engineering*, CPE-POWERENG, Florence, Italy / Virtual Conference, 14-16 July 2021, 6 pp.

[42] J. Peralta, H. Saad, S. Dennetiere, J. Mahseredjian and S. Nguefeu, "Detailed and Averaged Models for a 401-Level MMC–HVDC System," in *IEEE Transactions on Power Delivery*, vol. 27, no. 3, pp. 1501-1508, July 2012

Eros B. Avdiaj was born in Tirana, Albania, in 1995. He received the M. Sc (cum laude) degree in electrical engineering from Politecnico di Milano, Italy, in 2020. He is currently working toward a Ph.D. degree in harmonic and stability assessment of future grid-forming converters at KU Leuven/ EnergyVille, Belgium.

In 2020 he performed his master's thesis research during an internship of ten months at SINTEF Energy Research, Trondheim, Norway, on the operation of grid-forming HVDC converters under unbalanced conditions. In March 2020, Mr. Avdiaj was part of the winning team in the ABB challenge in EV-charging. His research interest includes future power system dynamics, control, and modelling of power electronic converters.

Salvatore D'Arco received the M.Sc. and Ph.D. degrees in electrical engineering from the University of Naples "Federico II," Naples, Italy, in 2002 and 2005, respectively.

From 2006 to 2007, he was a postdoctoral researcher at the University of South Carolina, Columbia, SC, USA. In 2008, he joined ASML, Veldhoven, the Netherlands, as a Power Electronics Designer, where he worked until 2010. From 2010 to 2012, he was a postdoctoral researcher in the Department of Electric Power Engineering at the Norwegian University of Science and Technology (NTNU), Trondheim, Norway. In 2012, he joined SINTEF Energy Research where he currently works as a Senior Research Scientist. He is the author of more than 100 scientific papers and is the holder of one patent. His main research activities are related to control and analysis of power-electronic conversion systems for power system applications, including real-time simulation and rapid prototyping of converter control systems.

Luigi Piegari (M'04-SM'13) was born in Naples, Italy, on April 2, 1975. He received the M.S. (cum laude) and Ph.D degrees in Electrical Engineering from the University of Naples Federico II, Italy, in 1999 and 2003, respectively.

He was, from 2003 to 2008, a Postdoctoral Research Fellow in the Department of Electrical Engineering, University of Naples Federico II, Italy. From 2009 to 2012, he was assistant professor at Department of Electrical Engineering of the Polytechnic University of Milan. He is currently associate professor of Electrical Machines and Drives at the Department of Electronics, Information and Bioengineering of the Polytechnic University of Milan. He is the author of more than 130 scientific papers published in international journals and conference proceedings. His research interests include storage devices modelling, wind and photovoltaic generation, modelling and control of multilevel converters and DC distribution grids.

Prof. Piegari is a member of the IEEE Industrial Electronics Society, of the IEEE Power Electronics Society and of AEIT. He is associate editor of the IEEE Journal of Emerging and selected topics in industrial electronics and technical program chair of the International Conference on Clean Electrical Power.

Jon Are Suul (M'11) received the M.Sc. degree in energy and environmental engineering and the Ph.D. degree in electric power engineering from the Norwegian University of Science and Technology (NTNU), Trondheim, Norway, in 2006 and 2012, respectively.

From 2006 to 2007, he was with SINTEF Energy Research, Trondheim, where he was working with simulation of power electronic converters and marine propulsion systems until starting his Ph.D. studies. Since 2012, he has been a Research Scientist with SINTEF Energy Research, first in a part-time position while working as a part-time Postdoctoral Researcher with the Department of Electric Power Engineering of NTNU until 2016. Since August 2017, he has been an Adjunct Associate Professor with the Department of Engineering Cybernetics, NTNU. His research interests are mainly related to modelling, analysis, and control of power electronic converters in power systems, renewable energy applications, and electrification of transport.